

and a HexNAc residue, suggesting that the glycan in the m/z 966.0²⁺ glycopeptide was linked to the peptide through HexNAc rather than DATDH (Fig. 4C, inset). In view of the DATDH synthesis pathway (19), it is likely that the HexNAc-linked oligosaccharide represents a precursor of the DATDH oligosaccharide (fig. S1).

A number of *C. jejuni* N-linked glycoproteins, whose glycosylation is dependent on the *pgl* gene cluster, have been identified (6). These glycoproteins have diverse functions in the cell but are all located extracytoplasmically. This is in agreement with the periplasmic space being the proposed site of PglB-mediated glycosylation in *C. jejuni*. The composition of the oligosaccharide did not show similarities to the highly conserved Glc₃Man₅GlcNAc₂ oligosaccharide that is transferred to protein in the ER of eukaryotes. However, as in eukaryotes, the protein-bound oligosaccharide in *C. jejuni* was linked to the amide nitrogen of asparagine within the consensus sequence Asn-Xaa-Ser/Thr. This sequence is essential for N-linked protein glycosylation in eukaryotes, and it has been proposed that it forms a specific secondary structure, the Asn-turn, recognized by the oligosaccharyltransferase (10). The presence of this consensus sequence on glycoproteins of *C. jejuni* suggests that the reaction mechanisms in eukaryotes and in *C. jejuni* are very similar. It is proposed that PglB fulfills the oligosaccharyltransferase function in the prokaryote and that Stt3 protein represents the catalytic subunit of the eukaryotic oligosaccharyltransferase complex. With the bipartite nature of the eukaryotic N-glycosylation pathway in mind, we speculate that in *C. jejuni* the heptasaccharide is assembled in the cytoplasm on a lipid carrier, most likely bactoprenyl pyrophosphate, translocated to the periplasmic side of the membrane, and transferred to protein (fig. S1).

To our knowledge, a general N-glycosylation system very similar to the one found in eukaryotes has not been described in other bacteria, and the *C. jejuni* genome is the only bacterial genome sequenced to date that harbors a gene that encodes a protein with strong sequence homology to a eukaryotic oligosaccharyltransferase component. The unique biosynthetic potential of *C. jejuni* and the isolated appearance of such an oligosaccharyltransferase ortholog in this organism led us to conclude that lateral gene transfer (20) of the oligosaccharyltransferase gene either from the archaeal or the eukaryal domain is responsible for this unique biosynthetic property of *C. jejuni*.

Note added in proof: The structure of the N-linked glycan of *C. jejuni* has recently been published (21).

References and Notes

1. C. Schäffer, M. Graninger, P. Messner, *Proteomics* **3**, 248 (2001).
2. I. Benz, M. A. Schmidt, *Mol. Microbiol.* **45**, 267 (2002).

3. P. R. Erickson, M. C. Herzberg, *J. Biol. Chem.* **268**, 23780 (1993).
4. R. Kornfeld, S. Kornfeld, *Annu. Rev. Biochem.* **54**, 631 (1985).
5. C. M. Szymanski, R. Yao, C. P. Ewing, T. J. Trust, P. Guerry, *Mol. Microbiol.* **32**, 1022 (1999).
6. D. Linton, E. Allan, A. V. Karlyshev, A. D. Cronshaw, B. W. Wren, *Mol. Microbiol.* **43**, 497 (2002).
7. R. Zufferey et al., *EMBO J.* **14**, 4949 (1995).
8. R. Knauer, L. Lehle, *Biochim. Biophys. Acta* **1426**, 259 (1999).
9. S. Silberstein, R. Gilmore, *FASEB J.* **10**, 849 (1996).
10. B. Imperiali, K. L. Shannon, M. Unno, K. W. Rickert, *J. Am. Chem. Soc.* **114**, 7944 (1992).
11. E. Bause, G. Legler, *Biochem. J.* **195**, 639 (1981).
12. D. Karaoglu, D. J. Kelleher, R. Gilmore, *Biochemistry* **40**, 12193 (2001).
13. See Supporting Online Material on Science Online.
14. Single-letter abbreviations for the amino acid residues are as follows: A, Ala; C, Cys; D, Asp; E, Glu; F, Phe; G, Gly; H, His; I, Ile; K, Lys; L, Leu; M, Met; N, Asn; P, Pro; Q, Gln; R, Arg; S, Ser; T, Thr; V, Val; W, Trp; and Y, Tyr. X indicates any residue.
15. P. Kotyczka, M. Wacker, M. Aebi, unpublished data.
16. H. R. Morris et al., *Rapid Commun. Mass Spectrom.* **10**, 889 (1996).
17. P. Teng-umnuay et al., *J. Biol. Chem.* **273**, 18242 (1998).
18. E. Stimson et al., *Mol. Microbiol.* **17**, 1201 (1995).
19. P. M. Power et al., *Microbiology* **146**, 967 (2000).
20. W. F. Doolittle, *Trends Cell Biol.* **9**, M5 (1999).
21. N. M. Young et al., *J. Biol. Chem.* **277**, 42530 (2002).
22. B. N. Fry et al., *Microbiology* **144**, 2049 (1998).
23. B. Dornon, C. E. Costello, *Glycoconjugate J.* **5**, 397 (1988).
24. We thank P. Guerry for providing us with *C. jejuni* 81-176 strain and plasmid containing AcrA, B. N. Fry for plasmid pBTLPS, and D. G. Newell for providing antibodies raised against *C. jejuni* whole-cell extracts. Supported by grants from the Swiss National Science Foundation to M.A. and by grants from the UK Biotechnology and Biological Sciences Research Council and the Wellcome Trust to B.W.W., H.R.M., and A.D.

Supporting Online Material

www.sciencemag.org/cgi/content/full/298/5599/1790/DC1

Materials and Methods

Fig. S1

References and Notes

24 July 2002; accepted 17 September 2002

Structural Adaptations in a Membrane Enzyme That Terminates Endocannabinoid Signaling

Michael H. Bracey,^{1*} Michael A. Hanson,^{2*} Kim R. Masuda,¹ Raymond C. Stevens,^{2,3†} Benjamin F. Cravatt^{1,2,4†}

Cellular communication in the nervous system is mediated by chemical messengers that include amino acids, monoamines, peptide hormones, and lipids. An interesting question is how neurons regulate signals that are transmitted by membrane-embedded lipids. Here, we report the 2.8 angstrom crystal structure of the integral membrane protein fatty acid amide hydrolase (FAAH), an enzyme that degrades members of the endocannabinoid class of signaling lipids and terminates their activity. The structure of FAAH complexed with an arachidonyl inhibitor reveals how a set of discrete structural alterations allows this enzyme, in contrast to soluble hydrolases of the same family, to integrate into cell membranes and establish direct access to the bilayer from its active site.

Several amidated lipids serve as endogenous signaling molecules in the mammalian central nervous system, modulating behaviors such as pain, cognition, feeding, sleep, and locomotor activity (1–5). A subset of these, including anandamide (1), bind to the central cannabinoid receptor CB1, a heterotrimeric GTP-binding protein (G protein)-coupled receptor activated by the psychotropic component of marijuana, Δ^9 -THC (6). Additional classes of lipid transmitters have also emerged as regulators of nervous system function (7). Nonetheless, the molecular mechanisms for regulating lipid-based signal-

ing events remain largely unknown. Although classical neurotransmitters can be confined spatially by membrane-delineated compartments for controlled storage, release, and uptake, lipid messengers are not easily contained by such physical boundaries. Because lipids can readily partition to and diffuse throughout cell membranes, termination of their signaling capacity may rely primarily on chemical transformation, possibly within the bilayer itself, instead of on cellular uptake and compartmentalization.

The amplitude and duration of fatty acid amide signals are regulated in vivo primarily by a single degradative enzyme, the integral membrane protein fatty acid amide hydrolase (FAAH) (8). Transgenic mice lacking FAAH possess high endogenous concentrations of anandamide and related fatty acid amides in the brain that correlate with increased CB1-dependent analgesia in these animals (9), suggesting that FAAH may represent an at-

Departments of ¹Cell Biology, ²Chemistry, and ³Molecular Biology, ⁴Skaggs Institute for Chemical Biology, Scripps Research Institute, 10550 North Torrey Pines Road, La Jolla, CA 92037, USA.

*These authors contributed equally to this work.

†To whom correspondence should be addressed. E-mail: cravatt@scripps.edu, stevens@scripps.edu

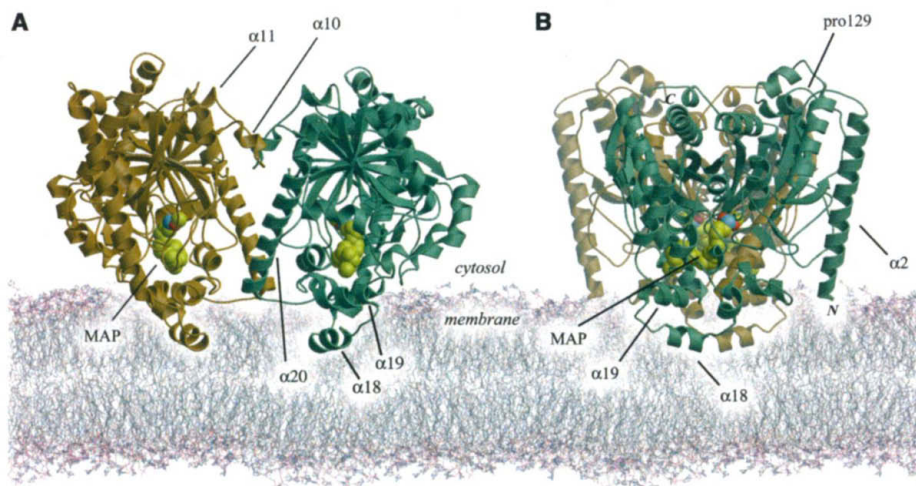


Fig. 1. Structure of the integral membrane protein FAAH modeled into a lipid bilayer. The enzyme is a homodimer assembled from 63-kD subunits. The inhibitor adduct MAP is depicted in the active site with van der Waals surfaces rendered in yellow (carbon), gray (phosphorus), and red (oxygen). **(A)** Front view of the enzyme, highlighting the central twisted β sheet that forms the core of the structure. **(B)** Side view produced by a 90° rotation from the view in **(A)**. The amino (N) and carboxyl (C) termini of the green subunit are labeled; Pro¹²⁹ is indicated. A genetic polymorphism conferring substitution of threonine at this position has been implicated in drug abuse and renders the enzyme more vulnerable to proteolytic attack (25). All figures were produced with Molscript (26), GRASP (23), and Raster3D (27). The membrane model was generated by a Molecular Dynamics simulation of a palmitoyloleoylphosphatidylethanolamine (POPE) bilayer (28).

tractive therapeutic target for treating pain and related neurological disorders. FAAH is the only characterized mammalian member of the amidase signature (AS) superfamily of serine hydrolases (10); other members are soluble enzymes that hydrolyze hydrophilic substrates such as acetamide (11), malonamide (12), and glutamine (13). Relative to other AS enzymes, two distinguishing features of FAAH are its integration into membranes and its strong preference for hydrophobic substrates (14). To elucidate the structural basis for these unique biochemical properties, we determined the three-dimensional structure of FAAH to 2.8 Å resolution by x-ray crystallography. Coordinates and structure factors have been deposited in the Protein Data Bank (accession code 1MT5).

We obtained protein crystals by recombinantly expressing rat FAAH with 29 amino acids deleted at the NH₂-terminus. Although the deleted region is predicted to participate in membrane binding (8), the truncated FAAH variant (residues 30 to 579) retains the wild-type protein's association with membranes, detergent requirement for solubilization, and ability to degrade fatty acid amides in mammalian cells (15). Crystals of FAAH

Table 1. Summary of data collection and refinement statistics. Initial phases were calculated with DmMulti (24), incorporating all MAD and MIRAS contributions. Ramachandran distributions of amino acids in the final model were calculated with PROCHECK (24) from a single protein

chain after phase refinement under tight NCS restraints. Side chains for which no density was observed were set to zero occupancy during refinement, and no σ -based rejection of reflections was used.

	Twin		MAD		
Data set	T1	Ta peak	Ta inflection	Os peak	Remote
Beam line	ALS 5.0.2	SSRL 9-2	SSRL 9-2	SSRL 9-2	SSRL 9-2
Wavelength (Å)	0.97910	1.255	1.2554	1.14025	0.925
Space group	<i>P</i> 2 ₁	<i>C</i> 222 ₁	<i>C</i> 222 ₁	<i>C</i> 222 ₁	<i>C</i> 222 ₁
Resolution (Å)	50 to 2.8	65 to 3.3	65 to 3.3	60 to 3.3	48 to 3.3
Unique reflections	173,615	81,567	81,574	81,609	81,511
Redundancy	2.1	14.5	14.5	14.5	14.5
Completeness*	76 (79)	99.7 (99.1)	99.7 (99.2)	99.8 (99.5)	99.7 (98.7)
<i>I</i> /(σ) [*]	4.4 (2.7)	8.2 (2.3)	6.9 (1.2)	7.6 (1.7)	8.5 (2.2)
<i>R</i> _{sym} (%) [*]	10.4 (26.4)	7.9 (33.3)	9.7 (63.2)	8.5 (45.5)	7.4 (33.4)

Phasing from Ta₆Cl₁₂·OsCl₃ MAD data

Resolution (Å)	96 to 3.3
Number of Os sites	8
Number of Ta sites	0
Os peak isomorphous phasing power (centric/acentric)	0.948/1.43
Os peak anomalous phasing power (acentric)	2.18
Remote isomorphous phasing power (centric/acentric)	0.288/0.471
Remote anomalous phasing power (acentric)	1.88
Ta inflection anomalous phasing power (acentric)	0.871
Ta peak (reference) anomalous phasing power (acentric)	1.02

Combined figure of merit before NCS and multicrystal averaging (3.3 Å) (centric/acentric) 0.47/0.60

Twinning operator (*l*, $-h$, *k*)
Twinning factor (α) 0.28

Refinement against detwinned data set T1

Resolution (Å)	50–2.8
Reflections used	173,615
Test reflections	9,297
Number of nonhydrogen atoms	65,120
<i>R</i> _{work} (%)	20.0
<i>R</i> _{free} (%)	23.7
Average <i>B</i> value (Å ²)	44.829
MAFP average <i>B</i> value (Å ²)	64.26
RMSD bond length (Å)	0.029
RMSD bond angle (°)	1.041

Ramachandran distributions (%)

Most favored	82.6
Additionally allowed	15.5
Generously allowed	1.5
Disallowed†	0.4

*Numbers in parentheses refer to data in the highest resolution shell. †Of the 16 chains in the asymmetric unit, only Glu¹²² was consistently in a disallowed region, and this residue falls on the *i* + 1 position of a γ turn. Complete data collection and refinement statistics are available as supporting online material (table S1). MAFP, methoxy arachidonoyl fluorophosphonate; RMSD, root mean square deviation.

complexed with methoxy arachidonyl fluoro-phosphonate, an active site-directed irreversible inhibitor, were obtained in three space groups: twinned $P2_1$ with 16 molecules in the asymmetric unit, $C222_1$ with 8 molecules in the asymmetric unit, and $P6_322$ with 2 molecules in the asymmetric unit (16). We first determined the structure of the FAAH-inhibitor complex to 3.3 Å by using a combination

MIRAS/MAD (multiple isomorphous replacement with anomalous signals/multi-wavelength anomalous diffraction) phasing strategy followed by phase extension with multicrystal and NCS (noncrystallographic symmetry) averaging (Table 1). The resulting electron density maps displayed density for more than 90% of the side chains with no main-chain breaks, yielding an exceptional

search model for molecular replacement phasing of twinned monoclinic data. The final model, built in $P2_1$ at 2.8 Å resolution, was of excellent quality.

The crystal structure of FAAH reveals a dimeric enzyme (Fig. 1), consistent with chemical cross-linking studies indicating that the enzyme is a dimer in solution (15). The dimer interface buries about 1560 Å² of molecular surface area per monomer (17). The protein core is characterized by a twisted β sheet consisting of 11 mixed strands, which is surrounded by 24 α helices of various lengths. The overall fold of the monomer closely resembles that of malonamidase (MAE2) from the nitrogen-fixing bacterium *Bradyrhizobium japonicum*, the only other AS enzyme for which a structure is available (12). However, there are key structural differences.

We identified the active site of FAAH on the basis of the location of core catalytic residues defined previously by mutagenesis (10, 18) and from the density of the inhibitor adduct methoxy arachidonyl phosphonate (MAP) (Fig. 2). The catalytic nucleophile Ser²⁴¹ is covalently bonded to the phosphorus of the MAP molecule, and the neighboring density can be modeled to accommodate the arachidonyl chain in an energetically favorable conformation (Fig. 2A). As observed for MAE2, the serine nucleophile in FAAH forms part of an unusual Ser-Ser-Lys catalytic triad with Ser²¹⁷ and Lys¹⁴² (Fig. 2B), and the relative orientation of the catalytic residues is nearly superimposable between the structures of FAAH and MAE2 (root mean square deviation = 0.27 Å). In contrast, the substrate binding pockets of FAAH and MAE2 differ significantly. The tunnel leading from the surface of FAAH and containing the buried arachidonyl chain is lined with a preponderance of aromatic and aliphatic amino acids (Fig. 2B), many of which arise from sequence insertions in FAAH relative to MAE2. These residues include Ile⁴⁹¹, identified by ultraviolet crosslinking and mutagenesis studies to participate in substrate recognition (14). In contrast, the active site of MAE2 is lined with mostly hydrophilic amino acids that accommodate its soluble substrate, malonamide (12).

Amino acids 410 to 438, another sequence insertion in FAAH relative to MAE2, form a helix-turn-helix motif that interrupts the AS fold. The two helices α18 and α19 cap the active site and present several hydrophobic residues that likely constitute FAAH's membrane binding face (Figs. 1 and 3A). The NH₂-terminus of the intact enzyme, predicted by sequence analysis to form an additional membrane binding helix (amino acids 7 to 29), would be properly positioned to reinforce the membrane interactions of the α18 and α19 membrane cap (Fig. 1B).

A potential substrate entryway is adjacent to

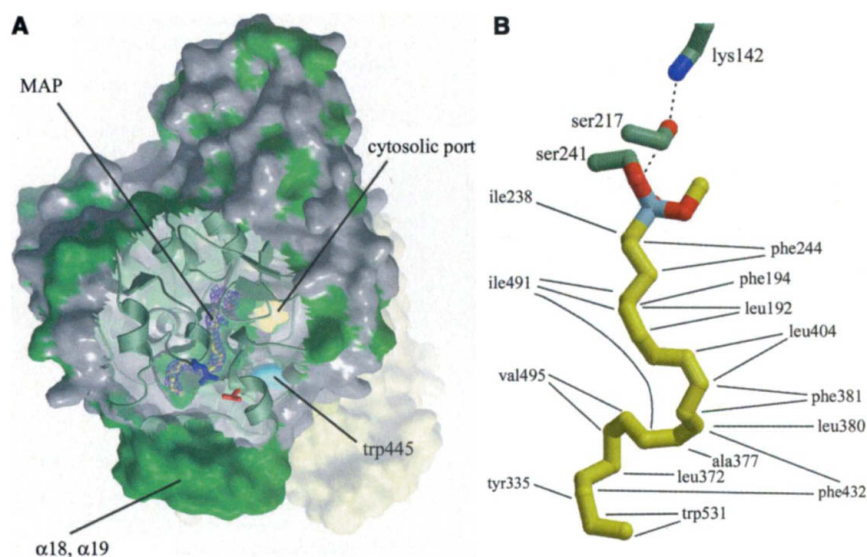


Fig. 2. Active site of FAAH in complex with the arachidonyl inhibitor MAP. (A) FAAH dimer is shown with the protein surface rendered in gray (hydrophilic) and green (hydrophobic) for one subunit and in pale yellow for its mate. A portion of the protein surface has been removed to highlight the continuous internal channel leading from the membrane binding face at Arg⁴⁸⁶ (blue) and Asp⁴⁰³ (red) to the active site and on to the cytosolic port. Electron density corresponding to the arachidonyl inhibitor is shown in violet and lies in the hydrophobic (green) substrate binding pocket. Trp⁴⁴⁵ from the dimer mate is rendered in van der Waals surface and is colored cyan to demonstrate the effective plugging of this potential port. (B) Aromatic and aliphatic residues in the substrate binding pocket surrounding the arachidonyl chain and their interactions are indicated. Also shown is the unusual Ser-Ser-Lys catalytic triad of FAAH (Ser²⁴¹-Ser²¹⁷-Ser²⁴¹), with the Ser²⁴¹ nucleophile covalently bonded to the phosphorus atom of the MAP inhibitor.

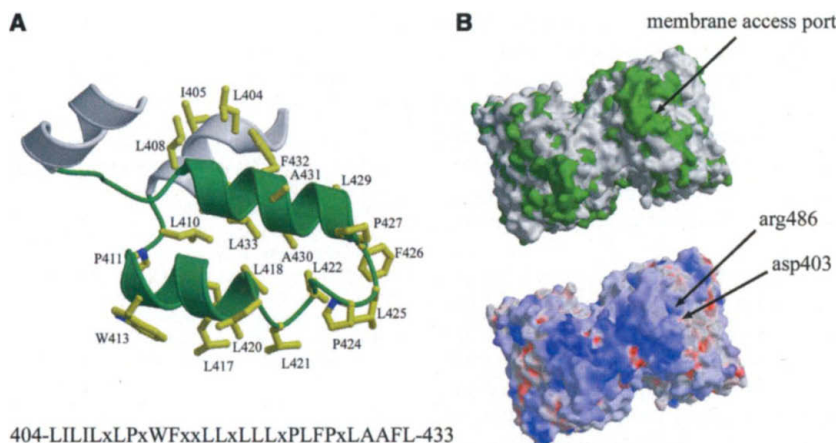


Fig. 3. Predicted membrane binding cap of FAAH. (A) Hydrophobic helices α18 and α19 that constitute the putative membrane binding cap are shown in green. The primary sequence of this domain (404 to 433) is indicated by single-letter code (29), except for hydrophilic amino acids, which are indicated by x. Five of these seven hydrophilic residues are Arg or Lys; the remaining two are Ser. (B) Molecular surface of FAAH viewed from the membrane face; the observed structure demonstrates the presence of a hydrophobic cap (top) (green), surrounded primarily by positive electrostatic potential (bottom) (blue, basic; red, acidic). The entrance to the active site from the membrane face is indicated, as are Arg⁴⁸⁶ and Asp⁴⁰³, which form one side of this access port.

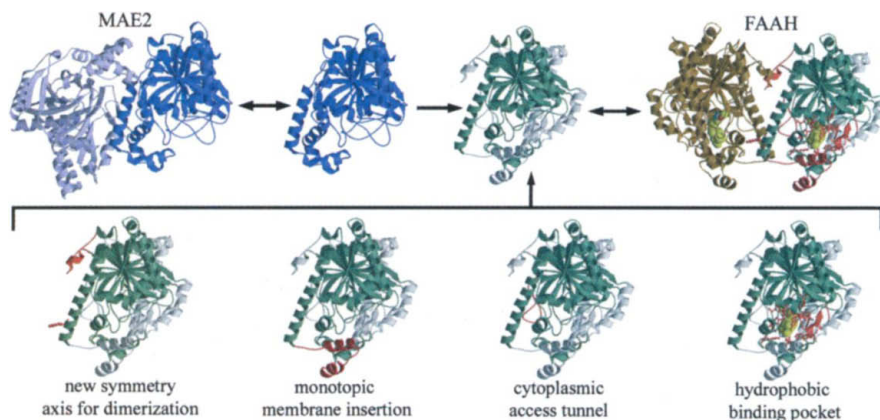


Fig. 4. Proposed modular adaptations that convert a soluble enzyme to an integral membrane enzyme, as inferred from differences in the structures of FAAH and MAE2. The soluble enzyme, if oligomeric, reorganizes so that all active sites can concurrently access the bilayer for maximal efficiency. The addition of discrete structural elements, represented here in red, confers the new oligomerization domain (Trp⁴⁴⁵ and residues 299 to 314) (lower left) as well as a membrane binding face (lower middle left) and cytoplasmic access channel (lower middle right). The final monotopic integral membrane enzyme must also undergo mutation of key substrate binding residues in the active site to effectively recruit its hydrophobic targets from the lipid bilayer (lower right).

$\alpha 18$ and $\alpha 19$, and the arachidonyl chain of MAP contacts Phe⁴³² of $\alpha 18$, which may indicate direct access between the FAAH active site and the hydrophobic membrane bilayer. The putative substrate entry is amphipathic in nature, with hydrophobic residues covering three sides of the rim and charged residues Arg⁴⁸⁶ and Asp⁴⁰³ completing the remaining side (Figs. 2A and 3B). This arrangement of residues may accommodate the admission and movement of polar fatty acid amide head groups toward the active site. Overall, the intimate relationship between the membrane binding surface and the active site of FAAH is similar to that of squalene cyclase (19) and prostaglandin H₂ synthase (20), which also act on lipid-soluble substrates and have hydrophobic caps surrounding their respective active site entrances. In all three enzymes, the hydrophobic cap is surrounded by basic amino acids (Fig. 3B) that may interact with negatively charged phospholipids.

A second major tunnel emerges from the active site at about an 80° angle from the arachidonyl-filled cavity. This tunnel bifurcates to create both a solvent-exposed cytosolic port and a route blocked by Trp⁴⁴⁵ (Fig. 2A), a residue that forms a lock-and-key intersubunit contact. Thus, the FAAH active site appears to simultaneously access both the aqueous environment of the cytoplasm and the lipid milieu of the bilayer. This architecture may provide an exit route to the cytosol for the polar amine substituents liberated from the fatty acid amide substrates and could also provide entry for a water molecule required for deacylation of the FAAH–fatty acyl intermediate (18).

A comparison of FAAH's structure with that of the soluble AS enzyme MAE2 reveals

how a single member of a large clade of proteins has adapted to perform a specialized cellular function through the addition of discrete folding modules and without gross changes in catalytic mechanism or fold architecture (Fig. 4). For example, although FAAH and MAE2 dimerize about roughly the same face, they have different relative monomer orientations. These distinct quaternary orientations produce an antiparallel and parallel alignment of the MAE2 and FAAH monomer active site entrances, respectively. The parallel orientation of FAAH monomers has important biological implications, because it should permit both subunits to function concurrently by recruiting substrates from the same membrane. Furthermore, this parallel alignment places another key structural module, the $\alpha 18$ – $\alpha 19$ hydrophobic cap, on the same face of the dimer, thereby enhancing membrane binding (Fig. 4). Additional sequence insertions in the FAAH protein account for other specialized features of the enzyme's structure, including its cytoplasmic channel and apolar substrate binding pocket (Fig. 4).

The intimate relationship between the active site of FAAH and cell membranes revealed by the enzyme's structure raises the possibility that fatty acid amides need not be transported through aqueous cellular compartments to proceed from site of action to site of degradation. As a consequence, proper endocannabinoid tone may rely on the expression levels of FAAH and its localization relative to cannabinoid receptor systems *in vivo* (21). Finally, the structure of FAAH may facilitate the design of inhibitors that could have therapeutic benefit for a variety of nervous system disorders (22), including not

only agents that bind to the enzyme acyl chain pocket but also compounds that target the active site via the cytoplasmic channel. The latter class of inhibitors might display exceptional selectivity for FAAH relative to the more than 100 lipid hydrolases present in the human proteome.

References and Notes

1. W. A. Devane *et al.*, *Science* **258**, 1946 (1992).
2. B. F. Cravatt *et al.*, *Science* **268**, 1506 (1995).
3. A. Calignano, G. La Rana, A. Guiffrida, D. Piomelli, *Nature* **394**, 277 (1998).
4. F. Rodriguez de Fonseca *et al.*, *Nature* **414**, 209 (2001).
5. A. H. Lichtman, E. G. Hawkins, G. Griffin, B. F. Cravatt, *J. Pharmacol. Exp. Ther.* **302**, 73 (2002).
6. R. I. Wilson, R. A. Nicoll, *Science* **296**, 678 (2002).
7. N. Fukushima, I. Ishii, J. J. Contos, J. A. Weiner, J. Chun, *Annu. Rev. Pharmacol. Toxicol.* **41**, 507 (2001).
8. B. F. Cravatt *et al.*, *Nature* **384**, 83 (1996).
9. B. F. Cravatt *et al.*, *Proc. Natl. Acad. Sci. U.S.A.* **98**, 9371 (2001).
10. M. P. Patricelli, M. A. Lovato, B. F. Cravatt, *Biochemistry* **38**, 9804 (1999).
11. K. Gomi, K. Kitamoto, C. Kumagai, *Gene* **108**, 91 (1991).
12. S. Shin *et al.*, *EMBO J.* **21**, 2509 (2002).
13. A. W. Curnow *et al.*, *Proc. Natl. Acad. Sci. U.S.A.* **94**, 11819 (1997).
14. M. P. Patricelli, B. F. Cravatt, *Biochemistry* **40**, 6107 (2001).
15. M. P. Patricelli, H. A. Lashuel, D. K. Giang, J. W. Kelly, B. F. Cravatt, *Biochemistry* **37**, 15177 (1998).
16. See supporting data on Science Online.
17. Buried van der Waals molecular surface area was calculated in GRASP (23).
18. M. P. Patricelli, B. F. Cravatt, *Biochemistry* **38**, 14125 (1999).
19. K. U. Wendt, K. Poralla, G. E. Schultz, *Science* **277**, 1811 (1997).
20. D. Picot, P. J. Loll, R. M. Garavito, *Nature* **367**, 243 (1994).
21. M. Egertova, D. K. Giang, B. F. Cravatt, M. R. Elphick, *Proc. R. Soc. London Ser. B* **265**, 2081 (1998).
22. D. L. Boger *et al.*, *Proc. Natl. Acad. Sci. U.S.A.* **97**, 5044 (2000).
23. A. Nicholls, K. Sharp, B. Honig, *Proteins Struct. Funct. Genet.* **11**, 282 (1991).
24. Collaborative Computational Project Number 4, *Acta Crystallogr.* **D50**, 760 (1994).
25. J. C. Sipe, K. Chiang, A. L. Gerber, E. Beutler, B. F. Cravatt, *Proc. Natl. Acad. Sci. U.S.A.* **99**, 8394 (2002).
26. P. J. Kraulis, *J. Appl. Crystallogr.* **24**, 946 (1991).
27. E. A. Merritt, D. J. Bacon, *Methods Enzymol.* **277**, 505 (1997).
28. D. P. Tieleman, H. J. C. Berendsen, *Biophys. J.* **74**, 2786 (1998) (<http://moose.bio.ucalgary.ca/download.html>).
29. Amino acids are identified by single-letter code: A, Ala; F, Phe; L, Leu; I, Ile; P, Pro; W, Trp.
30. We thank the staff at the Stanford Synchrotron Radiation Laboratories (SSRL), and especially P. Kuhn, for helpful discussions and technical assistance. We also thank SSRL and the Advanced Light Source for beam time and M. Patricelli for helpful discussions. Supported by NIH grant DA13173 (B.F.C.), the Searle Scholars program (B.F.C.), the Skaggs Institute for Chemical Biology, the Scripps Research Institute, National Research Service Award F32 MH12414-03 (M.H.B.), and a Jabinson graduate fellowship (M.A.H.).

Supporting Online Material

www.sciencemag.org/cgi/content/full/298/5599/1793/DC1
Materials and Methods
Table S1
Figs. S1 to S3

24 July 2002; accepted 25 September 2002